Ain Shams Engineering Journal (2013) 4, 593–604

Ain Shams University

Ain Shams Engineering Journal

www.elsevier.com/locate/asej
www.sciencedirect.com

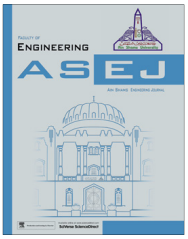

CIVIL ENGINEERING

Evaporation estimation for Lake Nasser based on remote sensing technology

Mohamed Hassan *

Nile Research Institute, National Water Research Center Building, El-Qanatir 13621, Egypt

Received 13 March 2012; revised 12 December 2012; accepted 17 January 2013
Available online 6 March 2013

KEYWORDS

Lake Nasser;
Evaporation;
Surface energy balance;
Remote sensing

Abstract Lake Nasser in Upper Egypt is of a great importance for Egypt as it represents a large reservoir for the country's freshwater resources. Precise studying of all elements contributing to the water balance of Lake Nasser is very crucial for better management of Egypt's water resources. Evaporation is considered an important factor of the water balance system that causes a huge loss of the lake's waters. In this study, evaporation rate for Lake Nasser is estimated using the surface energy balance approach based on remote sensing technology.

Evaporation rate obtained from this method is instantaneous since it is estimated during the satellite overpass over the lake. However, evaporative fraction method is used to estimate the daily rate from the instantaneous one. The surface energy balance combined with remote sensing data proves promising to estimate evaporation rates for large water bodies. These could lead to more accurate monitoring of evaporation rates in the lake area without being dependent on field observations, which are sometimes unavailable or uncertain for these types of studies.

© 2013 Ain Shams University. Production and hosting by Elsevier B.V.
All rights reserved.

1. Introduction

Lake Nasser is one of the largest artificial water reservoirs worldwide. The lake was created with the construction of Aswan High Dam 5 km upstream of Aswan city in Upper Egypt in 1964. Lake Nasser is located in an arid region in the south of Egypt. Evaporation is considered to be the most effective factor in understanding the water losses from the lake. Evaporation in Lake Nasser is of quite interest to many researchers and institutions in Egypt. For many years, the Egyptian Ministry of Water Resources and Irrigation adopted the figure of 7.54 mm/day as an annual mean evaporation rate with a maximum rate in June 10.8 mm/day, and a minimum in December 3.95 mm/day [1].

Understanding the physics of evaporation started early in the last century when Bowen [2] showed how available energy partitioning between latent heat flux and sensible heat flux could be determined using temperature gradients and humidity. Penman [3,4] mixed the energy balance concept with aerodynamic aspects of evaporation to develop an equation for estimating evaporation in 1948 that is widely adopted by water experts. In the next decades that follow, several theoretical and experimental models for evaluating evaporation techniques

* Tel.: +20 1003696964; fax: +20 242187152.
E-mail address: mohammedhasaneg@yahoo.com.
Peer review under responsibility of Ain Shams University

2090-4479 © 2013 Ain Shams University. Production and hosting by Elsevier B.V. All rights reserved.
http://dx.doi.org/10.1016/j.asej.2013.01.004

had been expanded. These included the Bowen Ratio Energy Budget (BREB) method and eddy-correlations techniques. These techniques are dependent on experimental data for verifications and the measurement of evaporation with equipment that evaluates the Bowen's ratio. A limitation of these techniques is that they yield essentially point values of evaporation, and therefore, are applicable only to a homogeneous area surrounding the equipment that is exposed to the same environmental factors [5]. Other methods to estimate evaporation rates include the water-budget method, methods of the so-called Dalton group such as the bulk aerodynamic or mass transfer method, methods in the so-called combination group such as Penman, Priestley–Taylor, and deBruin–Keijman methods, and methods in the temperature group such as the Papadakis method among others [6–8].

Most of the previous evaporation studies for Lake Nasser applied conventional methods, except Omar and El-Bakry [9] and Sadek et al. [10], who applied the BREB method, but with very limited data [11]. Elsawwaf et al. [11] compared results from six conventional methods for evaporation quantification with the values obtained by the BREB method based on calculations at the daily time scale covering a 10-year period (1995–2004). Evaporation rates of these conventional methods and the BREB method were estimated at the location of three meteorological floating stations data. Several of the six conventional methods showed substantial bias when compared with the BREB method. The conventional evaporation methods were adjusted to include the net energy advected term following the same procedure of Rosenberry et al. [12] to obtain close relation with the BREB values [11].

By the end of the last century, the Surface Energy Balance Algorithm for Land (SEBAL) was developed by Bastiaanssen et al. [13]. The model uses complex radiation and energy balance algorithms to estimate evapotranspiration from plants and soil. Ashfaque and Bastiaanssen [14] adopted the SEBAL technology in combination with remote sensing data to estimate evaporation for Lake Naivasha, Kenya. In this study, they compared daily evaporation rate based on evaporative fraction method and the surface energy balance approach with pan data based average evaporation estimation. In this study, daily estimation of evaporation was estimated using Landsat Thematic Mapper (TM) spectral data. The Landsat TM based estimation was compared with the pan data estimated average evaporation on the same date for the period of 1957–1990. Comparison between the two approaches to estimate evaporation showed reasonable results.

The application of the Simple Method [15] and surface energy balance approach using remotely-sensed data were applied to Rift Valley Lakes of Ethiopia. The Simple Method and a remote sensing-based lake evaporation estimates were compared to the Penman, Energy Balance, Pan, Radiation, and Complementary Relationship Lake Evaporation (CRLE) methods applied in the region [15]. Comparison of monthly Lake ET from the Landsat images to the Simple and Penman Methods showed that the remote sensing surface energy balance approach is promising for large scale applications to understand the spatial variation of the latent heat flux. Comparison of the lake evaporation estimates among lakes showed that Lake Langano, the mercky lake with high sediment loads, had lower average monthly evaporation than the other three lakes, which had less sediment loads, deeper and clearer than Lake Langano [15]. The presence of suspended sediment in lakes could lead to a higher surface temperature, and the higher near surface temperature can be related to a lower ET. This can be one of the weaknesses of the surface energy balance approach using thermal data from remote sensing [15].

The aim of this research is to evaluate evaporation rate estimates in Lake Nasser using the surface energy balance approach by adopting the SEBAL technology with Landsat TM spectral data of the lake. Evaporation estimates on several dates using the SEBAL technology and Landsat TM data were compared, and correlated with evaporation rates from six conventional methods. Monthly average evaporation estimates for the lake using the combination group methods such as the Penman, Priestley–Taylor, and deBruin–Keijman methods, the Mass Transfer method, the Papadakis method, and BREB method were obtained for the study dates from the research conducted by Elsawwaf et al. [11].

2. Study area and data

Lake Nasser was created after the construction of Aswan High Dam in 1964 south of Aswan city passing through the Egyptian Sudanese borders. The lake has a surface area of about 6500 km^2 and a length of about 500 km. The lake is formally divided into two lakes, one of length 350 km in Egypt, which is called Lake Nasser and the other of length 150 km located in Sudan, and is called Lake Nubia. The Egyptian part of the Lake lies between latitudes 22°00′N and 23°58′N, and longitudes 31°07′E and 33°15′E. The main source of water supply to the lake comes from the watersheds at the equatorial lakes and the Ethiopian plateau. This study is focusing on the Egyptian part of the lake. The surface area of the lake is changing according to the water discharges in the lake and the annual amount of flood. The lake has an average width of 10 km and a maximum width of 60 km and an average depth of 25 m and a maximum depth of 90 m. Field trip missions used to be organized by Nile Research Institute (NRI) to take samples and to observe several parameters of the lake related to sedimentation, water quality, etc. These observations are usually made at some specific cross sections across the Lake.

Three automatic floating stations belong to the High Aswan Dam Authority were installed in 1995. The three stations are located upstream of the Aswan High Dam (AHD), at Raft 2 km, Allaqi 75 km, and Abu-Simble 280 km (Fig. 1). Each floating system is recording hourly data of maximum, minimum and mean air temperature, relative humidity, surface water temperature, 2 m depth water temperature, wind speed, and wind direction. The three stations are working with full capacity since 1995 for the stations at Raft and Allaqi, and from 2000 for the station at Abusembel.

In this study, seven Landsat images in the period from October 1998 to October 2000 (Table 1) were used for the estimation of latent heat flux and lake evaporation. For the study dates, only meteorological data of the Raft station were available.

3. SEBAL methodology

3.1. Instantaneous estimation

In the surface energy budget approach (Fig. 2) for a deep lake or reservoir, latent heat flux, LE, sensible heat flux, H, change

Figure 1 Location map of the Nasser Lake area showing the floating stations (FSs) sites and the major physical features of Lake Nasser.

Table 1 Parameters values used in SEBAL estimation process at Raft station.

Date	Air temp. (T_a) (at 2 m) °C	Wind speed (u) (at 2 m) m/s	Q_x (w/m^2)	Q_v (w/m^2)
October 15-1998	30.3	4	−50	40
November 16-1998	22.4	5.5	−50	10
January 19-1999	12.8	2.2	−50	−5
November 03-1999	21.9	1.1	−50	23
March 17-2000	17.8	1.7	10	−7
June 14-00	33.8	3.9	50	−23
October 04-2000	27	1.2	−20	60

in energy stored, Q_x, and net energy advected, Q_v, can be related to the net radiation according to the following equation [16]:

$$R_n - H - \mathrm{LE} = Q_x - Q_v \tag{1}$$

where R_n is net radiation (W m^{-2}) at the water surface, H is sensible heat flux (W m^{-2}), E is evaporation (m s^{-1}), L is latent heat of vaporization (J kg^{-1}), LE is latent heat flux (W m^{-2}) required for evaporation, Q_x is the increase in energy stored in the water body (W m^{-2}), and Q_v is the net energy advected into the water body because of inflowing and outflowing water (W m^{-2}). The latent heat flux LE can be calculated as a residual from the last equation, where R_n is positive when radiation is received by the water surface, and H, and LE are positive when they are emitted by the water surface.

Net radiation R_n can be calculated from the incoming and outgoing all wave radiation fluxes. R_n can be expressed in its constituent elements as:

$$R_n = (1 - r_o) \times K\downarrow + \sigma\varepsilon_a T_a^4 + (1 - \varepsilon_o) \times \sigma\varepsilon_a T_a^4 - \sigma\varepsilon_o T_o^4 \tag{2}$$

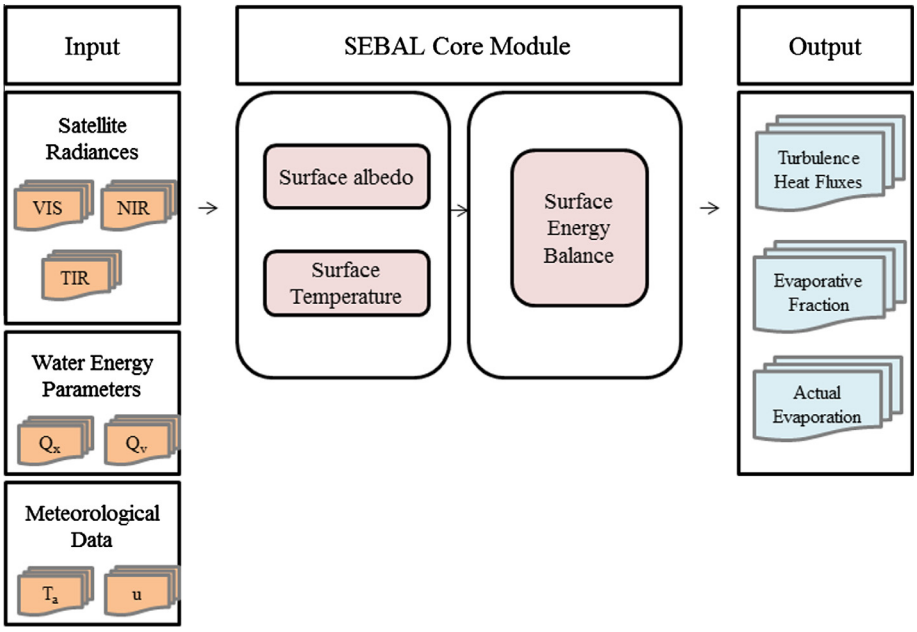

Figure 2 Principal components of the Surface Energy Balance for Land for Lake Nasser which converts remotely measured spectrally emitted and reflected radiances into the surface energy balance and evaporation indicators.

where r_o is surface albedo, $K\downarrow$ is the down welling shortwave radiation (W m^{-2}), $\sigma = 5.67 \times 10^{-8}$ is the Stephan's Boltzman constant (W m^{-2} K^{-4}), ε_a, ε_o and T_a (K), T_o (K) are the emissivity and temperature of the air and water surface respectively. Details of the derivation of the components of the net radiation exchange can be found in Bastiaanssen et al. [13]. From Eq. (1), the latent heat flux LE (W m^{-2}) can be estimated as a residual in other parameters of the algorithm as:

$$\mathrm{LE} = R_n - H - Q_x + Q_v \tag{3}$$

The sensible heat flux H can be defined as a part of the surface energy that is used to heat up the planetary boundary layer [14]. Based on the theory of mass transport of heat and momentum between surface and near surface, Bastiaanssen et al. [13] suggested a mathematical formulation for H as:

$$H = \frac{\rho_a C_p}{r_{\mathrm{ahsur}}}(T_o - T_a) \tag{4}$$

where $\rho_a \approx 1.2$ (kg m^{-3}) is the air density, $C_p \approx 1004$ (J kg^{-1} k^{-1}) is the specific heat of moist air, T_o is the water surface temperature, T_a is the air temperature at 2 m height, and r_{ahsur} is aerodynamic resistance to heat transport (s m^{-1}) and can be estimated as:

$$r_{\mathrm{ahsur}} = \frac{1}{K^2 u}(\ln(Z/Z_o))^2 \tag{5}$$

where K is Von Karman's constant ($K = 0.41$) (–), u is velocity of air [m s^{-1}], Z is observation height (m), and Z_o is the water surface roughness length ($Z_o = 0.00137$) (m). The aerodynamic resistance to heat transport r_{ahsur} is very high because of negligibly small water surface roughness. In case of Lake Nasser, there is usually a difference in temperatures between water surface and air at 2 m height. The difference between air and water surface temperatures will lead to a considerable portion of sensible heat flux (H).

The change in stored energy (Q_x) is an essential component of the energy budget because the large specific heat capacity of water allows even a small lake to store and exchange large amounts of heat energy [11]. Q_v is considered one of the most important inputs for the energy-budget approach for a large deep lake like Lake Nasser. Daily stored energy Q_x, and net advected energy, Q_v values for Lake Nasser were obtained from the study conducted by Elsawwaf et al. [11] for the time periods of this study (Table 1).

3.2. Daily evaporation estimation

The evaporative fraction Λ (–) is the ratio of the energy used for the evaporation process divided by the total amount of energy available for the evaporation process and can be expressed mathematically as:

$$\Lambda_{\mathrm{inst}} = \frac{\mathrm{LE}}{\mathrm{LE} + H} = \frac{\mathrm{LE}}{R_n + Q_v - Q_x} \tag{6}$$

Evaporation from open-water bodies is quite different from these above land surfaces [17]. The sun's energy penetrates the water to depths of as much as 30 m in clear water, somewhat less in turbid water, and is stored throughout the water column [17]. The water column is mixed by surface motion and becomes the source of energy that drives evaporation [17]. Because of the large heat storage capacity of water (1.006×10^6 J m^{-3}) and the fact that water is approximately 1000 times more dense that air, the temperature of deep, clear, water bodies does not change significantly throughout the day when compared to the atmosphere [17]. The amount of available energy at the surface is nearly constant throughout the day and night, leading to a nearly constant evaporation rate [11].

In SEBAL, the evaporative fraction Λ in Eq. (6) is assumed constant during daytime hours. Experimental work has shown that this holds true for environmental conditions where surface

moisture does not significantly change. The evaporative fraction remains unchanged during the day time and accordingly the instantaneous and the integrated daily evaporation fraction can be considered the same; i.e. $\Lambda_{\text{inst}} = \Lambda_{24\text{Hours}}$ [18–20]. From Eq. (6) the daily evaporation $E_{24\text{Hours}}$ (mm/day) is calculated as:

$$E_{24\text{Hours}} = \frac{8.64 \times 10^7 \times \Lambda_{24\text{Hours}} \times (R'_n + Q'_v - Q'_x)}{\lambda \times \rho_w} \quad (7)$$

where λ is the latent heat of vaporization 2.45×10^6 [J kg^{-1}] (at a temperature 23 °C), ρ_w is the density of water 1000 [kg m^{-3}], R'_n is the daily net radiation (W m^{-2}), Q'_v is the daily net advected energy (W m^{-2}), and Q'_x is the daily change in stored energy (W m^{-2}). Values for Q'_v and Q'_x are given in Table 1. The daily net radiation R'_n can be calculated as:

$$R'_n = (1 - r_o) \times K\downarrow_{24\text{h}} + L_{n24\text{h}} \quad (8)$$

where $K\downarrow_{24\text{h}}$ and $L_{n24\text{h}}$ are the daily average incoming solar radiation and net long wave radiation respectively. An empirical formula to calculate $L_{n24\text{h}}$ was proposed by deBruin [21] as:

$$L_{n24\text{h}} = -110 \times \frac{K\downarrow_{24\text{h}}}{R_{a24\text{h}}} \quad (9)$$

where $R_{a24\text{h}}$ is the daily average extraterrestrial shortwave radiation (W m^{-2}) at the top of the atmosphere and $K\downarrow_{24\text{h}}/R_{a24\text{h}}$ is the daily average atmospheric shortwave transmittance. $K\downarrow_{24\text{h}}$ and $R_{a24\text{h}}$ were determined on the basis of standard astronomical equations [22].

4. Evaporation conventional methods

Six evaporation conventional methods were used for comparison with SEBAL method. These include;

a. The BREB [11] of Eq. (10) was developed for monthly estimation;

$$E_{\text{BREB}} = \frac{(R_n + Q_v - Q_x)}{\rho_w[L(1 + \text{BR}) + c(T_o - T_a)]} \times 8.64 \times 10^7 \quad (10)$$

Three of the so called combination methods, which quantify energy and advective terms;

b. Priestley Taylor method [23] of Eq. (11) was developed for periods of 10 days or greater estimation

$$E_{P-T} = \alpha \frac{S}{S + \gamma} \frac{R_n - Q_x}{L\rho_w} \times 8.64 \times 10^7 \quad (11)$$

c. deBruin–Keijman method [24] of Eq. (12) was developed for daily estimation;

$$E_{\text{dB}-K} = \frac{S}{0.85S + 0.63\gamma} \frac{R_n - Q_x}{L\rho_w} \times 8.64 \times 10^7 \quad (12)$$

d. Penman method [25] of Eq. (13) was developed for periods greater than 10 days;

$$E_{\text{Pen}} = \frac{S}{S + \gamma} \frac{R_n - Q_x}{L\rho_w} \times 8.64 \times 10^7 + \frac{S}{S + \gamma} \times (0.26(0.5 + 0.54U_2)(e_s - e_a)) \times 10^{-2} \quad (13)$$

On method of the Dalton group that requires measurement of several atmospheric parameters;

e. Mass Transfer method [26] of Eq. (14) that depends on calibration of N;

$$E_{M-T} = NU_2(e_o - e_a) \times 8.64 \times 10^7 \quad (14)$$

One method from the temperature group that requires only measurement of air temperature;

f. Papadakis method [27] of Eq. (15) was developed for monthly estimation;

$$E_{\text{Pap}} = 0.5625[e_s max \times 10^{-2} - (e_s min \times 10^{-2} - 2)] \times \frac{10}{d} \quad (15)$$

The multipliers 8.64×10^7 and 10 that appear in several equations are to convert output to mm/day,

BR Bowen ratio (dimensionless), c specific heat capacity of water (4186 J kg^{-1} °C^{-1}), α = 1.26 = Priestley–Taylor empirically derived constant, dimensionless, S = slope of the saturated vapor pressure–temperature curve at mean air temperature (Pa °C^{-1}), γ psychometric "constant" (depends on temperature and atmospheric pressure) (Pa °C^{-1}), ρ_w is the density of water 1000 [kg m^{-3}], U_2 wind speed at 2 m above water surface (m s^{-1}), N coefficient of efficiency of vertical transport of water vapor by eddies of the wind (used 1.458×10^{-11} Pa^{-1} for Nasser Lake as calculated by Omar et al. [9], e_s saturated vapor pressure at temperature of the air (Pa), e_o saturated vapor pressure at temperature of the water surface (Pa), e_a saturated vapor pressure at temperature and relative humidity of the air (Pa), d number of days in the month, $e_s max$ and $e_s min$ saturated vapor pressures at daily maximum and minimum air temperatures (Pa) [11].

5. Application

5.1. Remote sensing evaporation

In Section 3.1, remote sensing data can be used to solve for the parameters of r_o, and T_o in Eq. (2). Air temperature T_a at 2 m height above the water surface, and wind speed u are obtained from the meteorological data of the Raft station (Table 1) in order to estimate the sensible heat flux (H) in Eq. (4). Other parameters of Eq. (2) may be calculated from empirical equations.

According to the algorithm proposed by Bastiaanssen [28], at surface incoming shortwave radiation $K\downarrow$ can be estimated as:

$$K\downarrow = R_a\tau_{\text{sw}} \quad (16)$$

where R_a is the extra-terrestrial shortwave solar radiation (W m^{-2}), and τ_{sw} is the shortwave atmospheric transmittance (–). R_a and $K\downarrow$ were determined on the basis of standard astronomical equations [22]. The shortwave atmospheric transmittance τ_{sw} can be calculated from Eq. (16). Zhong and Li [29] proposed an equation to find τ_{sw} from local measurements and the two way transmittance τ''_{sw} for the broadband solar radiation (–);

$$\tau_{\text{sw}} = (\tau''_{\text{sw}})^{0.5} = ((r_p - r_a)/r_o)^{0.5} \quad (17)$$

where r_p is the broad band planetary albedo (–), r_a is the lowest planetary albedo at all pixels (–), and r_o is the surface albedo

(–). The approximate emissivity of the atmosphere ε_a is calculated according to Bastiaanssen [28] as:

$$\varepsilon_a = 1.08(-\ln \tau_{sw})^{0.265} \quad (18)$$

The broadband planetary albedo r_p can be calculated from multi spectral remote sensing data as:

$$r_p = \sum_{i=1}^{n} W_i r_p(_i) \quad (19)$$

where n is the total number of spectral bands, W_i is the weighting factor accounting for the uneven distribution of spectral incoming solar radiation at different bands, and $r_p(\lambda_i)$ is the spectral reflectance at the top of the atmosphere of band i (–). Landsat TM spectral measurements can be used to estimate r_p and T_o as will be shown in the next section. Surface albedo, r_o can be computed as a residual in Eq. (17).

5.2. Thematic mapper processing

Seven Landsat TM scenes were processed to estimate daily evaporation on the dates of the satellite overpass of each respective scene (Table 2). Landsat TM measures the spectral radiance at the top of the atmosphere for the visible, near infrared and thermal infrared of the spectrum. Digital Numbers DN were converted into radiance values at the top of the atmosphere using:

$$L_i = a + \frac{b-a}{255} * \mathrm{DN} \quad (20)$$

where $L_{\lambda i}$ (mW cm^{-2} sr^{-1} μm^{-1}) is the spectral radiance in band i of Thematic Mapper. The scaling parameters a, b and the spectral incoming solar radiation at the top of the atmosphere for the respective bands were obtained from the USGS page of Landsat calibration files [30]. The band wise spectral reflectance at the Top Of Atmosphere (TOA) for bands 1, 2, 3, 4, 5, and 7 were estimated using:

$$r_p(\lambda_i) = \frac{\pi L \lambda_i d_s^2}{K(\lambda_i)\cos\phi_{su}} \quad (21)$$

where $r_p(\lambda_i)$ is the spectral reflectance at the top of the atmosphere of band i (–), $d_s \approx 1$ is the earth sun distance in astronomical units, $K(\lambda_i)$ is the spectral incoming solar radiation (mW cm^{-2} sr^{-1} μm^{-1}), and ϕ_{su} is the sun elevation angle (deg.) for the respective scene. Broad band reflectance r_p (–) at TOA from all bands was estimated as:

$$r_p = \sum W_i r_p(_i) \quad (22)$$

where W_i are the weights for each band estimated as the fraction of the spectral incoming shortwave solar radiation of a certain band to the total spectral incoming solar radiation. Atmospheric correction was applied to the spectral emitted radiance of band 6 using:

$$CV_{r2} = \frac{\mathrm{CV_{r1}} - L\uparrow}{\varepsilon_o \mathscr{T}} + \frac{1-\varepsilon_o}{\varepsilon_o} L\downarrow \quad (23)$$

where $\mathrm{CV_{r2}}$ is the atmospherically corrected band 6 radiance (W m^{-2} sr^{-1} μm^{-1}), $\mathrm{CV_{r1}}$ is the uncorrected radiance (W m^{-2} sr^{-1} μm^{-1}), and ε_o is the water surface emissivity (typically 0.95). $L\downarrow$ down welling long wave radiance (W m^{-2}), $L\uparrow$ upwelling long wave radiance (W m^{-2}), and $\mathscr{T}$ Band average transmittance (–) are obtained from the atmospheric correction file of the respective scene according to the old meteorological data available at NASA [31]. Corrected radiance values were converted into water surface temperatures T_o in kelvin degrees using the inverse of Planck's function:

$$T_o = \frac{K_2}{\ln\left(\frac{K_1}{CV_{r2}} + 1\right)} \quad (24)$$

where K_1, K_2, are thermal constants obtained from the USGS page of Landsat calibration files [30]. The surface albedo, water surface temperature, instantaneous net radiation, instantaneous latent heat flux, evaporative fraction, and daily total evaporation from the lake were calculated using the surface energy balance approach (Fig. 2) for the seven Landsat TM scenes. Table 2 presents results of the SEBAL-based lake evaporation estimates. Figs. 3–8 show SEBAL Lake Nasser daily evaporation estimates on November 16, 1998 and their corresponding SEBAL spatial variables, instantaneous surface albedo (–), water surface temperature (K), instantaneous net radiation (W m^{-2}), instantaneous latent heat flux (W m^{-2}), and evaporative fraction (–) respectively.

6. Comparisons of SEBAL method with conventional methods

Some of the most commonly used evaporation methods were selected for comparison with the SEBAL method. SEBAL evaporation values on the study dates were compared to monthly evaporation rates of the same year at Raft station of the BREB method, the combination group methods such as the Penman, Priestley–Taylor, and deBruin–Keijman

Table 2 Comparison between SEBAL evaporation and conventional methods estimated evaporation.

Date	E_{SEBAL} (mm)	$E_{Priestley–Taylor}$ (mm)	$E_{deBruin–Keijman}$ (mm)	E_{Penman} (mm)	E_{BREB} (mm)	$E_{mass\ transfer}$ (mm)	$E_{Papadakis}$ (mm)
October 15-1998	7.15	13.8	14.0	11.2	11.8	11.6	10.6
November 16-1998	6.51	8.7	9.0	5.6	8.2	6.1	5.2
January 19-1999	5.5	5.8	6.2	3.7	6.2	5.2	6.2
November 03-1999	6.21	11.6	11.6	5.5	9.1	9.4	8.6
March 17-2000	5.8	5.0	5.1	2.6	5.1	4.9	5.0
June 14-2000	5.9	7.9	8.2	5.2	8.2	10.0	5.2
October 04-2000	9.1	12.2	12.2	9.7	8.2	8.1	5.7
Average	6.6	9.3	9.47	6.2	8.1	7.9	6.64
Correlation coefficient (r)	–	0.69	0.68	0.61	0.4	0.32	0.12

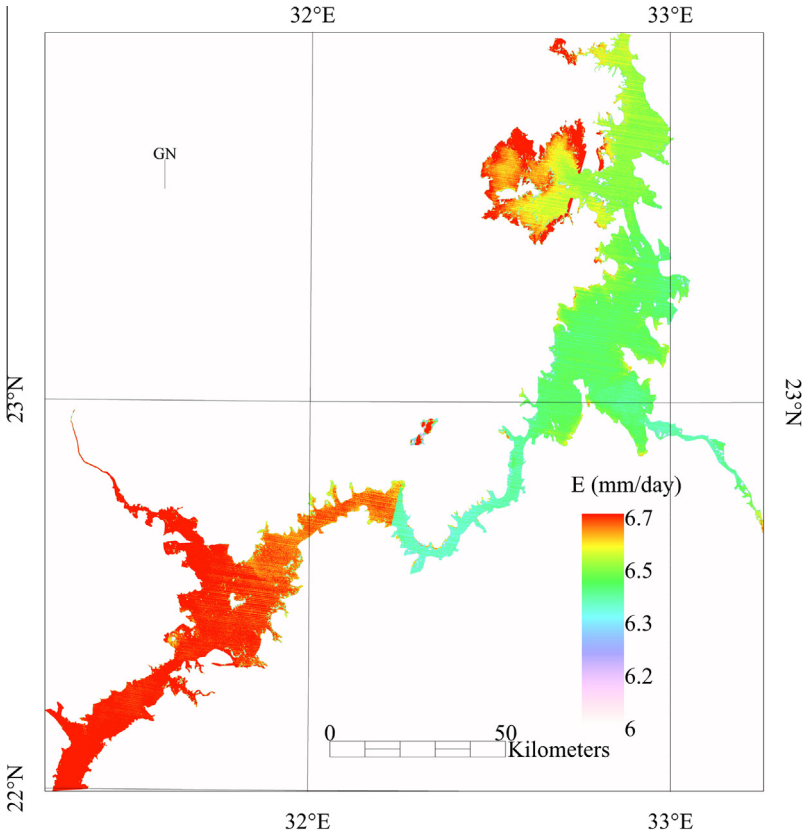

Figure 3 Daily evaporation rate of Lake Nasser (mm/day).

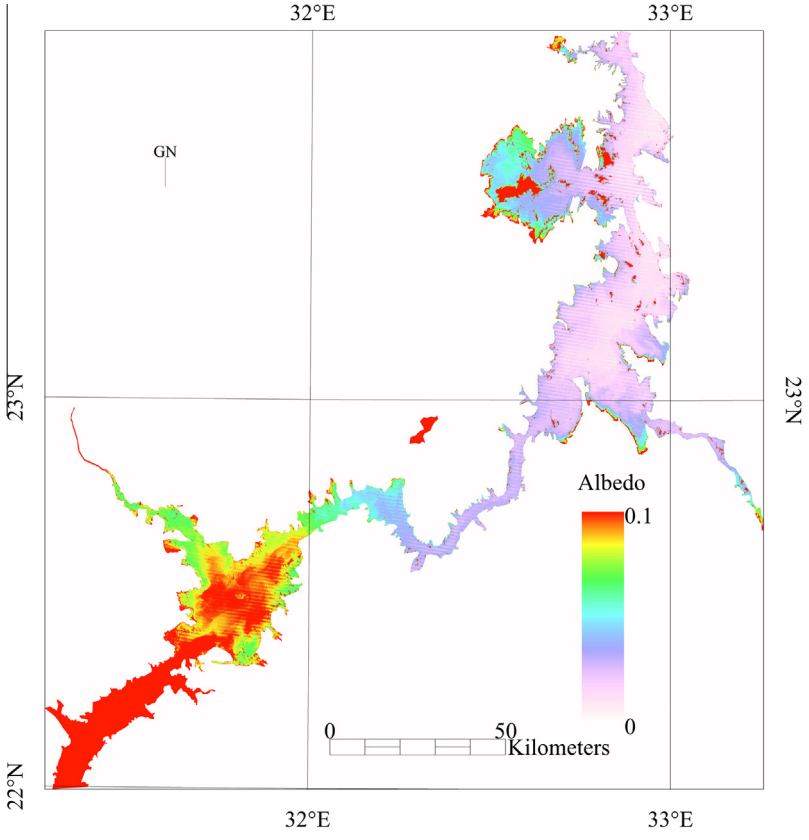

Figure 4 Instantaneous surface albedo (–).

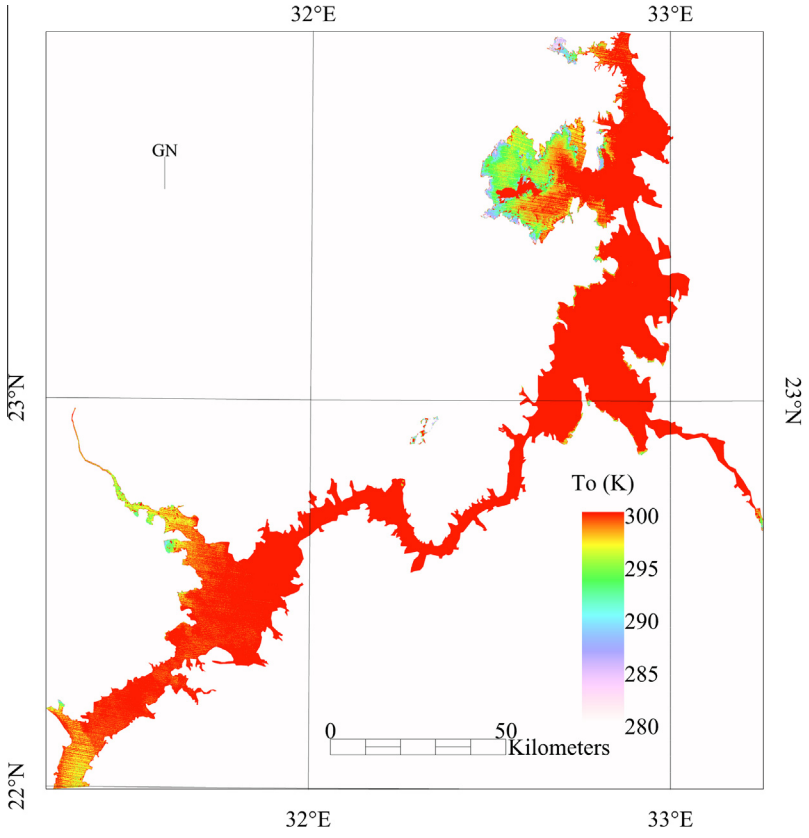

Figure 5 Water surface temperature at the time of satellite overpass (K).

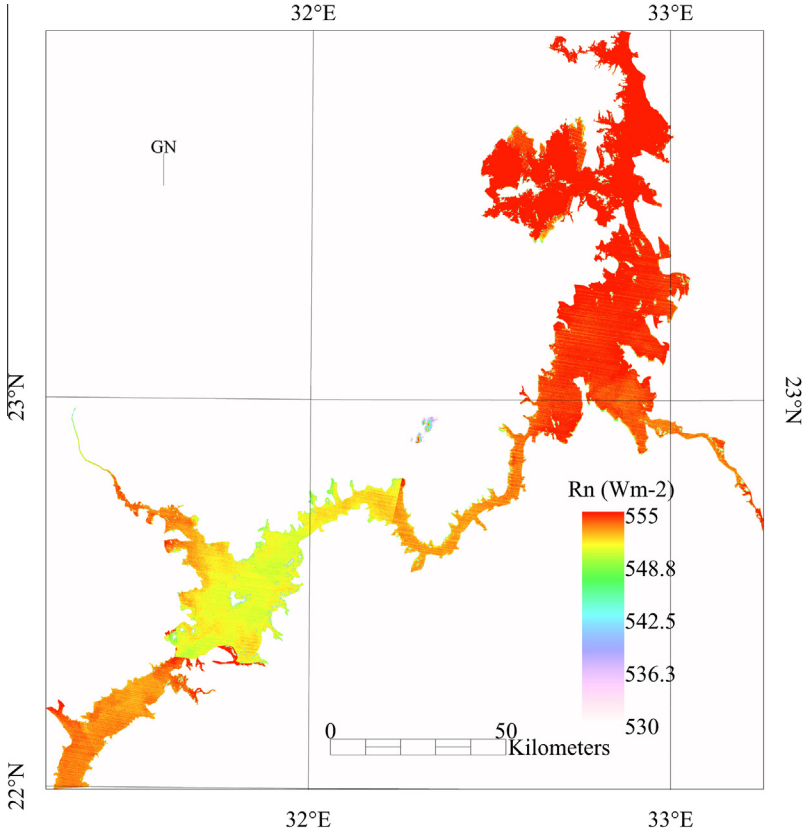

Figure 6 Instantaneous net radiation (W m^{-2}).

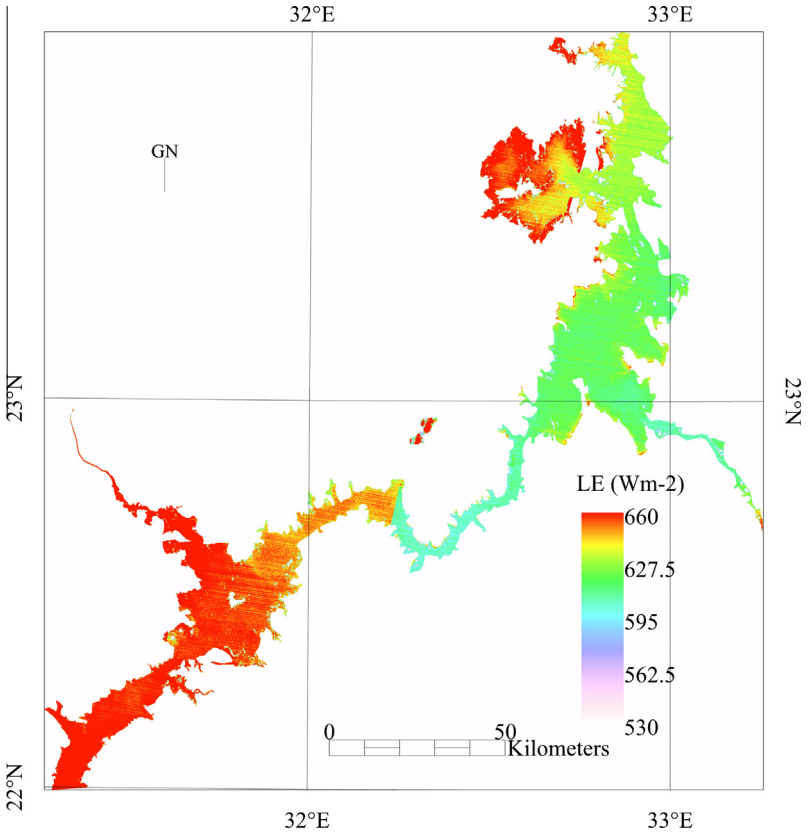

Figure 7 Instantaneous latent heat flux (W m^{-2}).

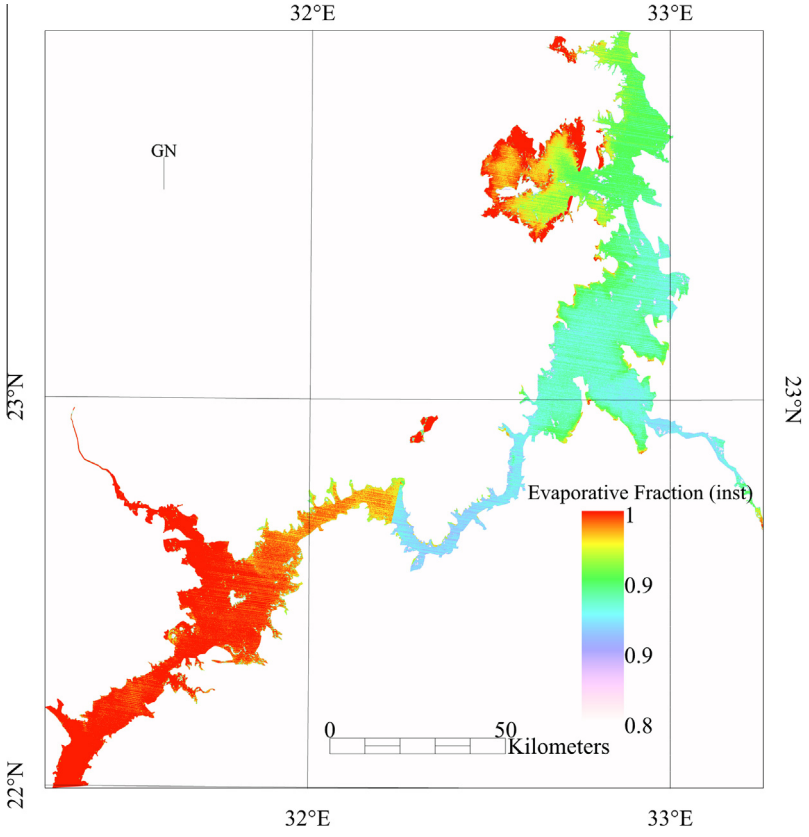

Figure 8 Evaporative fraction (–).

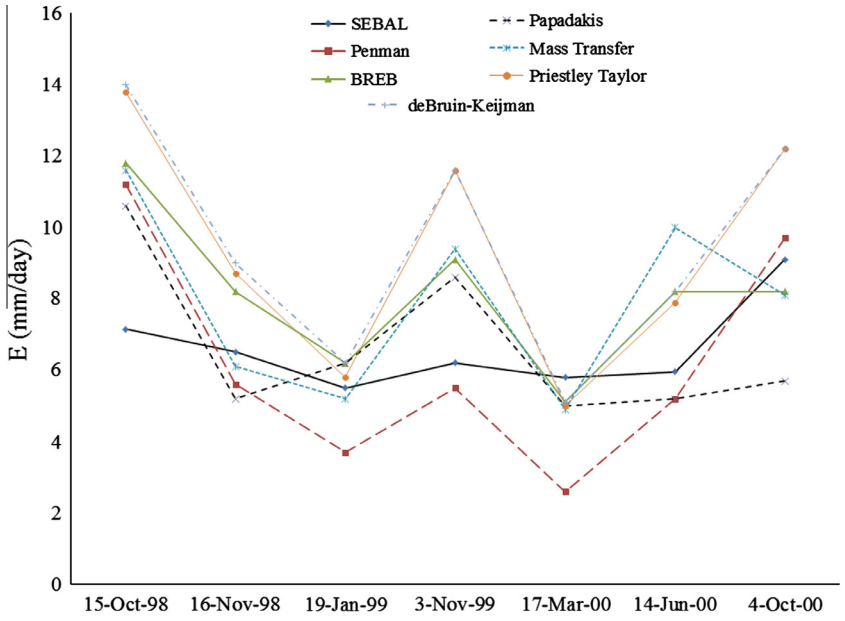

Figure 9 Graphical comparison of SEBAL evaporation with other conventional methods estimates.

methods, Papadakis method, and the mass transfer method (Section 4). Fig. 9 shows a graphical representation of the SEBAL evaporation estimates and evaporation estimates of other conventional methods on the study dates. Most of the used evaporation methods for comparison were developed to calculate potential evapotranspiration and they were used here to estimate evaporation from open water surface of Lake Nasser. As can be seen from Fig. 9, all evaporation methods have shown a large bias from SEBAL values during many of the study periods. This could be referred to the differences in performance of each evaporation method according to the physical condition of the lake on a certain date. It can be well noticed in Fig. 9 that differences between evaporation rates of the two combination group methods (Priestley Taylor and deBruin–Keijman) and SEBAL evaporation rates are greater during the flood months as in October and November for 1998 and in November 1999. Also, the difference between evaporation rates of these two methods and SEBAl evaporation is large during the month that proceeds and follows the flood season in July–September 2000. Differences in evaporation rates of these two methods and SEBAL rates are small during the rest of the periods as can be seen in January 1999 and March 2000. The BREB method has shown a similar behavior towards the SEBAL method as was the case with the two combination group methods (Priestley Taylor and deBruin–Keijman methods). The other combination group method (Penman method) did not show a specific behavior towards the SEBAL method during the flood season, but it has shown large negative evaporation rates differences during periods of normal flow such as in January 1999 and March 2000. Evaporation rates of the other two conventional methods (Mass Transfer and Papadakis methods) did not show a specific behavior towards the SEBAL method during the periods of normal flow but they did show a considerable high positive evaporation rates difference during months of the flood season such as in October 1998 and November 1999.

The results from the conventional evaporation methods were related to the SEBAL evaporation values using least-squares linear regression with SEBAL as the independent variable. As can be seen in Table 2, the three combination group methods (Priestley Taylor, deBruin–Keijman, and Penman) ranked best based on the correlation coefficient (r) criterion. Other conventional evaporation methods did not fit well with the SEBAL method based on the same criterion as they have shown small correlation coefficient (r). The Papadakis method has the worst correlation coefficient (r) to SEBAL method. Two of the conventional evaporation methods (Penman, and Papadakis) provided average evaporation values that were for the time periods of the study within 1 mm/day of the SEBAL values. The mass transfer and BREB methods provided average evaporation value within 1.5 mm/day of the SEBAL average evaporation estimation for the periods of the study.

The conventional evaporation methods also were ranked based on the percentage of monthly periods during which values from conventional methods differ less than 5%, 10%, and 20% of SEBAL values. The methods were ordered in Table 3 based on the 20% criterion. The Mass Transfer method has the first rank with 57% followed by the Penman and Papadakis methods with 57%. Based on the 20% criterion, the two combination group methods (Priestley Taylor and deBruin–Keijman) have the last rank. All conventional evaporation methods have large regression slope coefficient versus SEBAL. It can be well noticed from Table 3 that a high degree of correlation with the SEBAL values for the two combination group methods (Priestley Taylor and deBruin–Keijman) coincided with the smallest regression offsets. The good performance of the three methods of the combination group, which require the greatest number of measured input variables, indicates that evaporation methods that include available energy and aerodynamic terms provide the best comparisons with SEBAL evaporation at this station.

Although the mass transfer method has a low regression coefficient versus SEBAL, it has a relatively good regression slope coefficient and small regression offset versus SEBAL. Moreover, being at the first rank based on the 20% criterion highlights the fact that evaporation at this station is relevant

Table 3 Regression R^2, slope, offset coefficients for method output versus SEBAL values, and Percent of monthly periods that alternate evaporation values are within 5%, 10%, and 20% of SEBAL values for the study periods.

Alternate method	R^2 regressed against SEBAL	Regression slope coeff. versus SEBAL	Regression offset versus SEBAL	Results within 5% of SEBAL (%)	Results within 10% of SEBAL (%)	Results within 20% of SEBAL (%)
Raft station						
Mass transfer	0.10	0.68	3.38	14	28	57
Penman	0.37	2.02	−7.1	0	14	57
Papadakis	0.014	0.21	5.23	0	0	57
BREB	0.16	0.70	3.47	0	14	43
Priestley Taylor	0.48	1.90	−3.24	14	28	28
deBruin–Keijman	0.47	1.83	−2.62	0	0	28

to wind when the mass transfer method is applied. The method that requires measurements of only T_a, the Papadakis method, showed the worst correlation with SEBAL method based on the low regression R^2 coefficient and low regression slope coefficient. This indicates that this method is not well suited for use at Lake Nasser.

7. Conclusions

The Surface Energy Balance Algorithm for Land (SEBAL) to estimate daily evaporation rate was applied for a large lake like Lake Nasser in Upper Egypt. Latent heat flux, the main driving force for evaporation, is estimated as a residual in net radiation R_n, sensible heat flux H, change in stored energy Q_x, and net advected energy Q_v. The algorithm is applied to Landsat TM spectral data for the lake. Daily evaporation rates are estimated on seven different dates. Average monthly evaporation values of six traditional methods were compared with the SEBAL values at the Raft weather meteorological station. Evaporation methods that include available energy and aerodynamic terms (combination group methods) provide the best comparisons with the SEBAL evaporation. The good performance of the mass transfer method shows that evaporation at this location of the lake is very relevant to wind speed. On the contrary, the Papadakis method that depends on the measurement of air temperature is not suitable for application at Lake Nasser. Remote sensing based estimated latent heat flux with very limited hydro-meteorological data available from field observations is instrumental in estimating instantaneous rate of evaporation at the time of the satellite overpass. The daily total evaporation of the Lake is estimated using the evaporative fraction method based on the assumption that evaporation fraction remains unchanged over the day time for water surfaces. Future research in this field may apply the same concepts for other remote sensing data of higher temporal resolutions over longer study periods.

Acknowledgments

Support from Nile Research Institute (NRI) and fruitful discussions with colleagues are gratefully acknowledged and appreciated.

References

[1] Whittington D, Guariso G. Water management models in practice: a case study of the Aswan High Dam, Development in environmental modeling, 2. Amsterdam: Elsevier; 1983, p. 246.

[2] Bowen IS. The ratio of heat losses by conduction and by evaporation from any water surface. Phys Rev 1926;27:779–87.

[3] Penman HL. Natural evaporation from open water, bare soil and grass. Proc Royal Soc, London Ser A 1948;193:120–46.

[4] Penman HL. Evaporation in nature. Progress Phys 1948;11:366–88.

[5] Moran MS, Jackson RD. Assessing the spatial distribution of evapotranspiration using remotely sensed inputs. J Environ Qual 1991;20:525–737.

[6] Lenters JD, Kratz TK, Bowser CJ. Effects of climate variability on lake evaporation: results from a long-term energy budget study of Sparkling Lake, northern Wisconsin (USA). J Hydrol 2005;308:168–95.

[7] Winter TC. Uncertainties in estimating the water balance of lakes. Water Resour Bull 1981;17(1):82–115.

[8] Winter TC, Rosenberry DO, Sturrock AM. Evaluation of 11 equations for determining evaporation for a small lake in the north central United States. Water Resour Res 1995;31(4):983–93.

[9] Omar MH, El-Bakry MM. Estimation of evaporation from the lake of the Aswan High Dam (Lake Nasser) based on measurements over the lake. Agric Meteorol 1981;23:293–308.

[10] Sadek MF, Shahin MM, Stigter CJ. Evaporation from the reservoir of the high Aswan dam, Egypt: a new comparison of relevant methods with limited data. Theor Appl Climatol 1997;56:57–66.

[11] Elsawwaf M, Williams P, Pagano A, Berlamont J. Evaporation estimates from Nasser Lake, Egypt, based on three floating station data and Bowen ratio energy budget. Theor Appl Climatol 2010;100:439–65.

[12] Rosenberry DO, Winter TC, Buso DC, Likens GE. Comparison of 15 evaporation models applied to a small mountain lake in the northeastern USA. J Hydrol 2007;340:149–66.

[13] Bastiaanssen WGM, Menenti M, Feddes RA, Holtslag AAM. A remote sensing surface energy balance algorithm for land (SEBAL) 1. Formulation. J Hydrol 1998;212–213:198–212.

[14] Ashfaque A, Bastiaanssen WGM. Estimating evaporation from Lake Naivasha, Kenya using remotely sensed Landsat Thematic Mapper (TM) spectral data. J Civil Eng, The Institution of Engineers, Bangladesh, CE28-2; 2000.

[15] Melesse AM, Abtew W, Dessalegne T. Evaporation estimation of Rift Valley Lakes: comparison of models. Sens J 2009:9603–15, ISSN 1424-8220.

[16] Linsley RK, Kohler MA, Paulhus JLH. Hydrology for engineers. 2nd ed., McGraw-Hill series in water resources and environmental engineering; 1975. p. 155–8.

[17] Eichinger W, Nichols J, Prueger J, Hipps L, Neale C, Cooper D., et al. Lake evaporation estimation in arid environments. IIHR-Hydroscience & Engineering, The University of Iowa, IIHR, Report No. 430, 2003.

[18] Bastiaanssen WGM, Pelgrum L, Menenti M, Feddes RA. Estimation of surface resistance and Priestley–Taylor α-parameter at different scales. In: Stewart JB et al., editors. Scaling up in

hydrology using remote sensing. Wallingford: Institute of Hydrology. p. 93–111.
[19] Crago RD. Daytime evaporation from conservation of surface flux ratios. In: Stewart JB et al., editors. Scaling up in hydrology using remote sensing. Wallingford: Institute of Hydrology; 1996. p. 235–44.
[20] Shuttleworth WJ, Gurney RJ, Hsu AY, Ormsby JP. FIFE: the variation in energy partition at surface flux sites. IAHS Pub. No. 186, 1989, p. 67–74.
[21] deBruin HAR. From Penman to Makkink, Committee on Hydrological Research. TNO, The Hague Proceedings and Information 39-5-31; 1987.
[22] Iqbal M. An introduction to solar radiation. Canada: Academic press; 1983.
[23] Stewart RB, Rouse WR. A simple equation for determining the evaporation from shallow lakes and ponds. Water Resour Res 1976;12:623–8.
[24] deBruin HAR, Keijman JQ. The Priestley–Taylor evaporation model applied to a large, shallow lake in the Netherlands. J Appl Meteorol 1979;18:898–903.
[25] Brutsaert W. Evaporation into the atmosphere: theory, history, and applications. Dordrecht: D. Reidel; 1982, p. 299.
[26] Harbeck GE, Kohler MA, Koberg GE. Water-loss investigations: Lake Mead studies, U.S. Geological Survey Professional, paper 298; 1958.
[27] McGuinness JL, Bordne EF. A comparison of lysimeter-derived potential evapotranspiration with computed values. U.S. Department of Agriculture Agricultural Research Service, Washington DC, Technical, Bulletin 1452; 1972.
[28] Bastiaanssen WGM. Regionalization of surface flux densities and moisture indicators in composite terrain. A remote sensing approach under clear skies in mediterranean climates. Doctoral thesis, Wageningen Agricultural University, Wageningen, The Netherlands; 1995.
[29] Zhong Q, Li YH. Satellite observation of surface albedo over Qinghai–Xinzang plateau region. Adv In Atm Sci 1988;5:57–65.
[30] USGS Website. Landsat Calibration Data. <http://landsat.usgs.gov/science_calibration.php> [last accessed, January 2012].
[31] NASA Website. Atmospheric Correction Data. <http://atmcorr.gsfc.nasa.gov/> [last accessed, January 2012].

Dr. Mohamed Hassan is a Researcher at Nile Research Institute, National Water Research Center. He graduated from Zagazig University, Faculty of Engineering Shoubra and received his M.Sc. degree in 1990 and 1996, respectively. He obtained his Ph.D. in 2001 from Innsbruck University, Austria. His research interests focus on water resources engineering, and Geographic Information Systems.